Hydrogen Bonds between the α and β Subunits of the F_1-ATPase Allow Communication between the Catalytic Site and the Interface of the β Catch Loop and the γ Subunit†

Kathryn W. Boltz and Wayne D. Frasch*

Center for the Study of Early Events in Photosynthesis, Faculty of Biomedicine and Biotechnology, School of Life Sciences, Arizona State University, Tempe, Arizona 85287-4501

Received December 20, 2005; Revised Manuscript Received June 6, 2006

ABSTRACT: F_1-ATPase mutations in *Escherichia coli* that changed the strength of hydrogen bonds between the α and β subunits in a location that links the catalytic site to the interface between the β catch loop and the γ subunit were examined. Loss of the ability to form the hydrogen bonds involving αS337, βD301, and αD335 lowered the k_{cat} of ATPase and decreased its susceptibility to Mg^{2+}−ADP−AlF_n inhibition, while mutations that maintain or strengthen these bonds increased the susceptibility to Mg^{2+}−ADP−AlF_n inhibition and lowered the k_{cat} of ATPase. These data suggest that hydrogen bonds connecting αS337 to βD301 and βR323 and connecting αD335 to αS337 are important to transition state stabilization and catalytic function that may result from the proper alignment of catalytic site residues βR182 and αR376 through the VISIT sequence (α344−348). Mutations βD301E, βR323K, and αR282Q changed the rate-limiting step of the reaction as determined by an isokinetic plot. Hydrophobic mutations of βR323 decreased the susceptibility to Mg^{2+}−ADP−AlF_n inhibition and lowered the number of interactions required in the rate-limiting step yet did not affect the k_{cat} of ATPase, suggesting that βR323 is important to transition state formation. The decreased rate of ATP synthase-dependent growth and decreased level of lactate-dependent quenching observed with αD335, βD301, and αE283 mutations suggest that these residues may be important to the formation of an alternative set of hydrogen bonds at the interface of the α and β subunits that permits the release of intersubunit bonds upon the binding of ATP, allowing γ rotation in the escapement mechanism.

The F_1F_o ATP synthase uses the transmembrane proton gradient to drive the synthesis of ATP from ADP and P_i. The ATP synthase consists of the membrane-embedded F_o and the peripheral F_1.[1] When F_1 is isolated from F_o and the membrane, it is a soluble enzyme that can catalyze the hydrolysis of ATP. The F_1 from *Escherichia coli* is composed of five subunits with an $\alpha_3\beta_3\gamma\delta\epsilon$ stoichiometry. Of the six nucleotide binding sites located at the α−β interfaces of the $(\alpha/\beta)_3$ ring, three are catalytic sites, with the majority of the catalytic residues contributed by the β subunit, while the other three, located on the alternative α−β interfaces, are termed noncatalytic sites. Catalysis of ATP synthesis or hydrolysis occurs as the result of conformational charges induced by rotation of the central γ subunit within the $(\alpha\beta)_3$ ring that sequentially interacts with each of the three catalytic sites.

In the (ADP)(AMPPNP)F_1 crystal structure (*1*, *2*), the catalytic sites contain ADP and AMPPNP at the β_{DP} and β_{TP} sites, while the third catalytic site is empty (β_E). This structure may represent a low-energy ground state since structures with similar conformations have been derived under a variety of conditions, including one with a single Mg^{2+}−ADP−fluoroaluminate molecule present (*2*). The $(ADP{\cdot}AlF_4^-)_2F_1$ structure shows distinct conformational differences from the other structures and is unique in that all three catalytic sites are occupied by nucleotide (*3*). The long O−Al−O bond lengths and the presence of four fluorines of the bound fluoroaluminate suggest that the $(ADP{\cdot}AlF_4^-)_2F_1$ structure may represent a post-transition state intermediate structure. Because both (ADP)(AMPPNP)-F_1 and $(ADP{\cdot}AlF_4^-)_2F_1$ contain three heterodimers of subunits in related conformations, the three catalytic site conformations will be termed EA (β_E and α_E), FB (β_{TP} and α_{TP}), and DC (β_{DP} and α_{DP}) such that there are no presumptions about nucleotide occupancy in any conformation. The α−β heterodimer that was originally in the EA conformation progresses to FB, then to DC, and back to EA during three successive 120° γ subunit rotational events.

When a catalytic site is in the EA conformation (Figure 1A,E), γ subunit residues γR268[2] and γQ269 form hydrogen bonds and salt bridges to the catch loop of the β subunit (residues 301−305). It has been suggested that these hydrogen bonds prevent rotation until the nucleotide has bound to the catalytic site (*4*, *5*). The intersubunit hydrogen

† This work was supported by National Institutes of Health Grant GM50202 to W.D.F.

* To whom correspondence should be addressed. E-mail: Frasch@asu.edu. Telephone: (480) 965-8663. Fax: (480) 965-6899.

[1] Abbreviations: F_1, extrinsic membrane-associated protein of the F_1F_o ATP synthase; EF_1, F_1 portion of the *E. coli* F_1F_o ATP synthase; XL10, *E. coli* cell line containing γS193C, the six-His tag on the N-terminus of the α subunit, and deletion of an XmnI restriction site.

[2] *E. coli* residue numbers used throughout.

10.1021/bi052592+ CCC: $33.50
Published on Web 08/22/2006

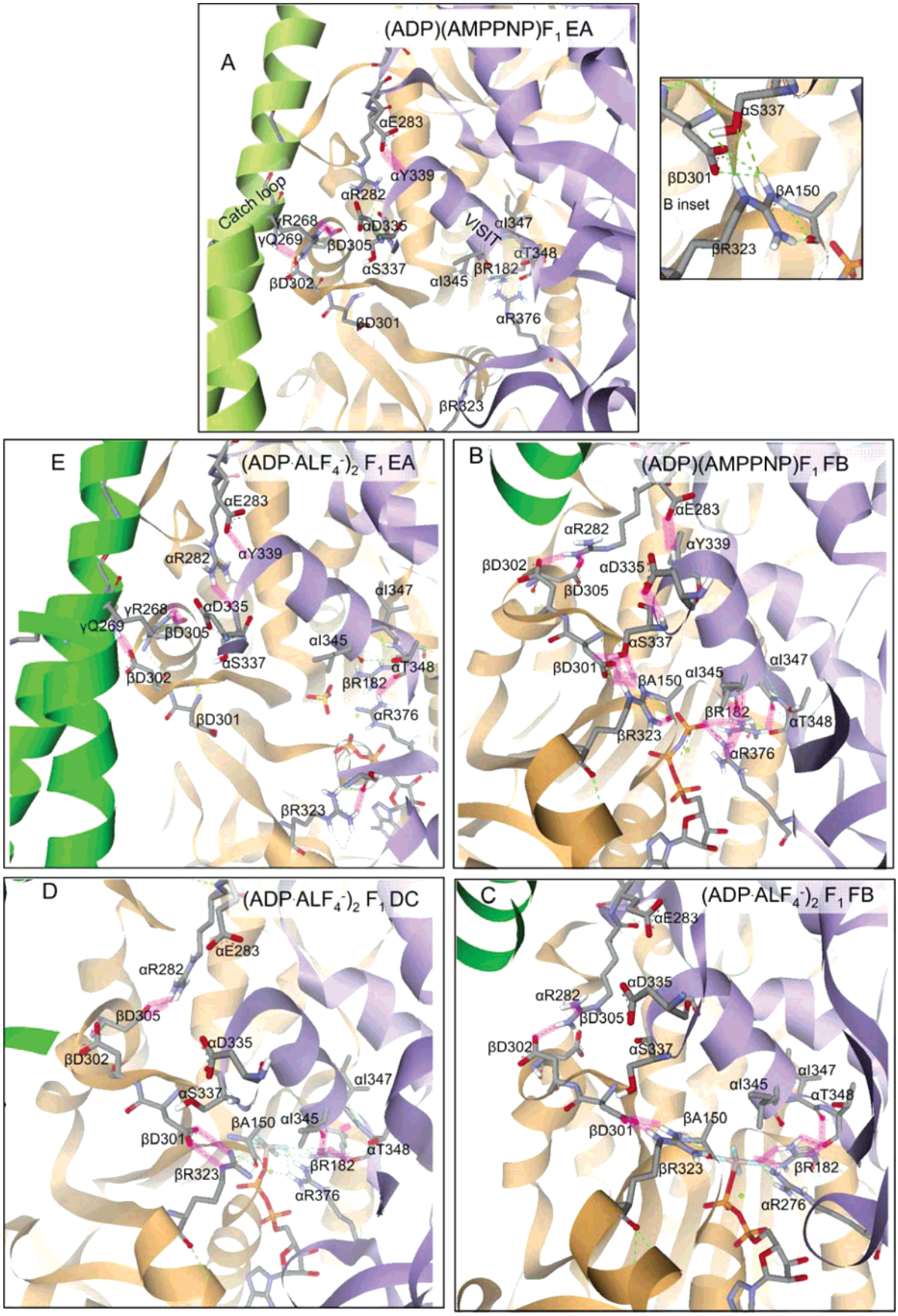

FIGURE 1: Interactions among the γ (green), α (purple), and β (orange) subunits. (A) (ADP)(AMPPNP)F_1 (*2*) in the EA conformation. (B) (ADP)(AMPPNP)F_1 in the FB conformation (inset, close-up of interactions of αS337, βD301, and βR323). (C) (ADP·AlF_4^-)$_2F_1$ (*2*) in the FB conformation. (D) (ADP·AlF_4^-)$_2F_1$ in the DC conformation. (E) (ADP·AlF_4^-)$_2F_1$ in the EA conformation. Bonds of interest are highlighted in pink. Crystal structure images are reproduced from Protein Data Bank entries 1E1Q and 1H8E using WebLab Viewer from Molecular Simulations, Inc.

Table 1: Primers Used To Generate Mutant Strains[a]

mutant strain	mutagenic primer (codon changes indicated)
αD335E	5′-gaaactcaggcgggtga**a**gtttctgcgttcgtt-3′
αD335N	5′-gaaactcaggcgggtca**a**gtttctgcgttcgtt-3′
αD335T	5′-gaaactcaggcgggt**ac**cgtttctgcgttcgtt-3′
αD335V	5′-gaaactcaggcgggtg**t**cgtttctgcgttcgtt-3′
αS337D	5′-caggcgggtgacgtt**ga**tgcgttcgttccgacc-3′
αS337C	5′-caggcgggtgacgttt**g**tgcgttcgttccgacc-3′
αS337V	5′-caggcgggtgacgtt**gt**tgcgttcgttccgacc-3′
αS337A	5′-gcgggtgacgtt**g**ctgcgttcgttccg-3′
βD301V	5′-cgtacctgcgg**t**tgacttgactgacccg-3′
βD301T	5′-gtatacgtacctgcg**ac**tgacttgactgacccg-3′
βD301N	5′-cgtacctgc**g**a**t**gacttgactgacccg-3′
βD301E	5′-cgtacctgcgga**g**acttgactgacccg-3′
βR323F	5′-gcaaccgtggta**ttt**agccgtcagatcgcg-3′
βR323K	5′-accgtggtactgagc**aaa**cagatcgcgtctctg-3′
βR323L	5′-ccgtggtactgagcc**t**tcagatcgcg-3′
βR323M	5′-accgtggtactgagc**atg**cagatcgcgtctctg-3′
αP289G/P290G	5′-ctgctgctccgtcgt**gg**g**gg**aggacgtgaagcattcccg-3′
αP289A/P290A	5′-ctgctgctccgtcgt**g**cg**g**caggacgtgaagcattcccg-3′
αR282E	5′-cgtcgtccgccagga**gaa**gaagcattcccgggc-3′
αR282Q	5′-cgtcgtccgccaggac**aa**gaagcattcccgggc-3′
αR282L	5′-ctccgtcgtccgccaggac**t**tgaagcattcccg-3′
αR282K	5′-ctccgtcgtccgccagga**aaa**gaagcattcccg-3′
αE283V	5′-ctgctgctccgtcgtccgccaggacgtg**t**agcattcccgggcgac-3′
αE283K	5′-ctgctgctccgtcgtccgccaggacgt**a**aagcattcccgggcgac-3′
αE283Q	5′-ctgctgctccgtcgccgccaggacgt**c**aagcattcccgggcgac-3′

[a] Codons containing changes are denoted with bold underlined text. Complementary primers (not shown) were also used in each mutagenesis reaction.

bonds and salt bridges connecting the catch loop of the β_E subunit to the γ subunit are critical to the function of the F_1 protein. Loss of ability to form these the $\beta-\gamma$ intersubunit bonds is devastating to enzyme activity (*5*).

In the FB conformation, the β subunit catch loop residues no longer interact with the γ subunit but instead make an alternate set of hydrogen bonds at the interface of the α and β subunits (Figure 1B and inset). Catch loop residues βD301, βD302, and βD305 form hydrogen bonds and/or salt bridges to βR323, αR282, and αS337, respectively. Additional hydrogen bonds and salt bridges form a continuous connection between the catch loop and residues βR182 and αR376, the arginine finger, that interact with the nucleotide at the catalytic site. This connection includes the αD335−αS337 and αE283−αY339 interactions. Residues αD335, αS337, and αY339 are connected by a short α helix to the conserved VISIT sequence, residues 344−348. In the FB conformation with bound MgAMPPNP (Figure 1B), catalytic residue βR182 is hydrogen bonded to VISIT residues αI345, αI347, and αT348, while the arginine finger, αR376, forms a hydrogen bond to αI345. These arginines are critical residues for the stabilization of the catalytic transition state (*6*−*8*) and the movement of phosphate away from ADP (*9*).

The catalytic residue known as the Walker B aspartate is connected to intersubunit γT273−βV265 and γE275−βV265 $\gamma-\beta$ hydrogen bonds through a short α helix (*1*−*3*). Eliminating or weakening these $\gamma-\beta$ intersubunit hydrogen bonds lowered the ATPase activity and decreased the sensitivity to Mg^{2+}−ADP−fluoroaluminate inhibition, while strengthening these intersubunit hydrogen bonds resulted in higher ATPase activity and more susceptibility to Mg^{2+}−ADP−fluoroaluminate inhibition than hydrophobic mutations (*10*). This was the first report of an intersubunit $\beta-\gamma$ interaction that was important to catalysis in its effect on the stability of the transition state.

We now report the effects of mutations that alter the hydrogen bonds that connect the β subunit catch loop to the catalytic site in the FB conformation. Mutations which eliminated the hydrogen bonds connecting catch loop residues βD301, αD335, and αS337 eliminated or significantly reduced ATP hydrolysis activity, as did mutations that affected the strength of the αE283−αY339 hydrogen bond. The results presented here indicate that these hydrogen bonds are important for catalytic function and stabilization of the catalytic transition state.

EXPERIMENTAL PROCEDURES

Strains and Plasmids. The parent plasmid and *E. coli* strain used in the this study are the same as those described previously (*5*). All site-directed mutagenesis for the current study was performed in plasmid pXL1 using the XL Quick Change Kit (Stratagene). The oligonucleotide primers for the creation of each mutant are shown in Table 1. The F_1-ATPase in the XL10 strain of *E. coli* contains a six-His tag on the α subunit and the γS193C mutation as described previously (*5*). Methods for culture growth and purification of EF_1 were carried out by following the method of Greene and Frasch (*5*). Growth yield in limiting glucose was measured through a modification of the procedure of Senior et al. (*11*). Growth of strains in 100 mL volumes of TDA with 3 mM glucose was followed through hourly optical density measurements. Reported values are based on the maximum optical density attained at 600 nm.

The rate of ATP hydrolysis was determined using an ATP-regenerating coupled assay that consisted of 50 mM Tris-HCl (pH 8.0), 10 mM KCl, 2.5 mM phosphoenolpyruvate, 0.15−0.3 mM NADH, 50 μg/mL pyruvate kinase, 50 μg/mL lactic dehydrogenase, and 3 nM F_1, with 2 mM Mg^{2+}−ATP. The rate was determined as a change in absorbance at 340 nm using a Cary 100 Bio UV−vis spectrophotometer

Table 2: Comparison of Oxidative Phosphorylation-Dependent Growth, and of ATP Hydrolysis[a]

strain	succinate-dependent doubling time (h)	succinate-dependent growth rate (% of that of XL10[c])	growth yield in limiting glucose (% of that of XL10)	k_{cat} (s^{-1}) for ATPase[d] (25 °C)	k_{cat} (% of that of XL10)
XL10	2.39	100	100	115	100
AN887	*b*	0	60	nd[e]	nd[e]
αD335V	3.98	60	76	22	19
αD335T	3.68	65	83	37	32
αD335N	3.27	73	90	31	27
αD335E	5.31	45	81	48	42
αS337A	2.28	105	96	88	77
αS337V	2.46	97	88	51	44
αS337C	2.54	94	96	48	42
αS337D	2.32	103	100	31	27
βD301V	4.05	59	79	0	0
βD301T	7.47	32	71	7	6
βD301N	4.19	57	82	150	130
βD301E	*b*	0	56	6	7
βR323L	1.93	124	114	103	90
βR323F	1.84	130	89	122	106
βR323M	4.89	49	80	76	66
βR323K	*b*	0	50	7	8
αP279G/P280G	2.08	122	118	32	28
αP279A/P280A	2.99	85	90	137	119
αR282L	2.57	93	96	99	86
αR282Q	2.52	95	97	15	13
αR282K	2.69	89	93	140	122
αR282E	*b*	0	64	0	0
αE283V	4.19	57	84	10	9
αE283Q	1.96	122	100	56	49
αE283K	4.42	54	80	5	4

[a] The culture did not double over the course of a 12 h period. [b] Measured as the slope at the log phase. [c] Standard deviations were <5%. The rates and relative abilities of purified F_1-ATPase to hydrolyze ATP at 2 mM Mg^{2+}−ATP at 25 °C are compared. [d] Not determined.

(Varian) equipped with a stir-controlled Peltier device. The reaction was initiated by the addition of F_1 to the assay mixture. Reaction rates were calculated from data collected 6−8 min after initiation of the reaction to allow for dissociation of the ϵ subunit and to minimize inhibition by entrapped Mg^{2+}−ADP (*12*). Inhibition of ATPase activity by the Mg^{2+}−ADP·AlF_n species was followed over time as described by Boltz and Frasch (*10*).

Activation energies and entropic and enthalpic components of the transition state for multisite ATP hydrolysis were calculated from measurements of maximal rates of ATPase activity as a function of temperature as described using eqs 1−3 (*13*):

$$E_A = \Delta H^{\ddagger} + RT \quad (1)$$

$$\Delta G^{\ddagger} = \Delta H^{\ddagger} - T\Delta S^{\ddagger} \quad (2)$$

$$\Delta G^{\ddagger} = -RT \ln(Nh/RTk_{cat}) \quad (3)$$

where E_A is the Arrhenius activation energy, T is the temperature, N is Avogadro's number, k_{cat} is the turnover number, and $\Delta H^{\ddagger}$ and $\Delta S^{\ddagger}$ are the enthalpic and entropic components of the changes in the Gibbs free energy of activation ($\Delta G^{\ddagger}$).

Membrane vesicles were prepared through a modification of the procedure of Futai et al. (*14*) as described by Boltz and Frasch (*10*). Fluorescence quenching was carried out as described by Boltz and Frasch (*10*). Formation of an electrochemical gradient was followed by suspending membrane vesicles in 2 mL of 50 mM Tris-HCl, 2 mM $MgCl_2$, 140 mM KCl, 1 μg/mL valinomycin, and 1 μM acridine orange (pH 8.0). The fluorescence at 530 nm (excitation at 490 nm) was monitored at room temperature with a stirred cuvette in a SPEX FluoroMax fluorometer. Fluorescence quenching was initiated by the addition of either 2 mM lactate to 10 mg of membranes or 2 mM ATP to 100 mg of membranes. The transmembrane proton gradient was collapsed by the addition of 2 μM carbonyl-cyanide-*m*-chlorophenylhydrazone (CCCP).

RESULTS

Effects of Mutations on ATP Synthase-Dependent Growth Rates and Enzyme Purity. Mutations were made to residues that contribute hydrogen bonds and salt bridges connecting the β catch loop to the catalytic residues βR182 and αR376 in the FB and DC states. The effects of these mutations on the function of ATP synthase were examined by measuring the growth rates on succinate and growth yields on limiting glucose (3 mM). *E. coli* strains XL10 and AN887, which does not express the enzyme due to a Mu phage suppression of the endogenous *unc* operon, were used as positive and negative controls, respectively. Table 2 summarizes doubling times from these ATP synthase-dependent growth experiments. All mutations to βD301 and αD335 and the αR282E, αE283V, αE283K, βR323M, and βR323K mutations eliminated or decreased the rate of ATP synthase-dependent growth. Hydrophobic βR323L and βR323F mutations increased the rate of ATP synthase-dependent growth, while βR323M and βR323K mutations decreased the rate of or eliminated ATP synthase-dependent growth.

The F_1-ATPase was purified from *E. coli* grown to late log phase on medium containing 30 mM glucose for all mutants that were examined. The yield of F_1 was consistent

Table 3: Comparison of Electrochemical Gradient Formation in Membranes from XL10 and Mutant Strains Measured by Fluorescence Quenching of Acridine Orange

strain	lactate-induced proton gradient (%)[a]	ATP-induced proton gradient (%)
XL10	100	100
αD335V	67	94
αD335T	69	98
αD335N	70	96
αD335E	112	98
αS337A	109	87
αS337V	67	86
αS337C	100	83
αS337D	95	23
βD301V	33	0
βD301T	87	0
βD301N	96	54
βD301E	92	0
βR323L	54	110
βR323F	88	43
βR323M	76	42
βR323K	34	9
αP279G/P280G	57	36
αP279A/P280A	42	85
αR282L	100	62
αR282Q	56	49
αR282K	83	38
αR282E	0	0
αE283V	70	62
αE283Q	96	77
αE283K	66	97

[a] The level of quenching was calculated by taking the difference between the maximum level of fluorescence quenching after the addition of lactate or ATP and the level after addition of 2 μM CCCP and then dividing by the value obtained for XL10 membranes.

between XL10 and all the mutant strains that were studied. The subunit composition of each preparation was analyzed by SDS−PAGE. In every case, the enyzme appeared pure and had the same subunit composition as XL10 (data not shown). These results indicate that the mutations did not significantly affect the synthesis and assembly of the enzyme and suggest that the change in growth rate on succinate for limiting glucose is the result of impaired F_1F_o synthase function.

Effects on Proton Gradient Formation with Inverted Vesicles. Mutant membranes were tested for the ability to generate a protonmotive force from lactate via electron transport (Table 3). Lactate-dependent fluorescence quenching was eliminated by αR282E, and the rate was reduced 3-fold by βD301V and βR323K. Mutations βR323L, αP279G/P280G, αP279A/P280A, and αR282Q reduced the level of lactate-dependent fluorescence quenching by 2-fold, while αD335V, αD335T, αD335N, αS337V, βR323M, αE283V, and αE283K reduced the level of quenching 25−33%. The remaining mutants did not affect lactate-dependent fluorescence quenching significantly.

ATPase-dependent proton gradient formation was assessed by fluorescence quenching of acridine orange using inverted membrane vesicles containing the F_1F_o ATP synthase (Table 3). ATPase-dependent fluorescence quenching was eliminated by βD301V, βD301T, βD301E, and αR282E, and the rate of quenching was reduced 10-fold by βR323K. Mutations αS337D, αP279G/P280G, and αR282K produced a 3−4-fold reduction in the level of ATPase-dependent fluorescence quenching, while βR323F, βR323M, αR282L, αR282Q, and αE283V reduced the level of quenching by ∼2-fold. Mutant αE283Q decreased the level of ATPase-dependent fluorescence quenching by ∼25%, while the other mutants had no effect.

Kinetic and Thermodynamic Analysis of F_1-ATP Hydrolysis Activity. Arrhenius plots of the Mg^{2+}−ATPase activity catalyzed by purified F_1-ATPase are shown in Figure 2. With the exceptions of those of αR282Q and αR282K, the Arrhenius plots remained linear up to 45 °C. Both αR282Q and αR282K were stable at 25 °C, and thus, a direct comparison of the effects of the mutants on k_{cat} was made at 25 °C (Table 2). ATPase activity was eliminated by βD301V and αR282E and reduced at least 10-fold by βD301T, βD301E, βR323K, αE283V, and αE283K. Mutations αR282Q, αD335V, αD335N, αS337D, and αP279G/P280G produced a 4−5-fold decrease in ATPase activity, while D335T, αD335E, αS337V, αS337C, and αE283Q produced a 2−3-fold decrease. Mutations αS337A and βR323M reduced ATPase activity by 25−33%.

From the slopes of the Arrhenius plots indicated by the solid lines in Figure 2, the values for enthalpy, entropy, and free energy of activation were calculated using eqs 1−3 at 25 °C (Table 4). The $\Delta G^{\ddagger}$ of XL10 at this temperature is 61.2 kJ/mol. Because the free energy of activation, $\Delta G^{\ddagger}$, is inversely proportional to k_{cat}, a k_{cat} value equivalent to that of XL10 can result from any combination of $\Delta H^{\ddagger}$ and $\Delta S^{\ddagger}$ due to eq 2 and the enthalpy−entropy compensation effect. Isobars representing the indicated percentage of the k_{cat} value of XL10 (Figure 3) were derived from the inverse relationship between k_{cat} and $\Delta G^{\ddagger}$. An enzyme will make and break many bonds, including hydrogen bonds, during a catalytic cycle. According to Eyring transition state theory, changes that result in a decrease in the level of bond interactions formed and broken during the rate-limiting step of the reaction will cause a shift to the lower left of the position of XL10, while changes that require more bond rearrangements will cause a shift to the upper right.

Shifts to the lower left of XL10 were observed with the mutations αP279A/P280A, αR282L, αR282Q, αE283V, αD335T, αD335E, αS337V, αS337C, αS337D, βD301N, βR323F, and βR323M, suggesting that fewer bonds needed to be made and broken during the rate-limiting step of the reaction with these mutants. Shifts to the upper right of XL10 were observed with the mutations αP279G/P280G, αR282K, αE283Q, αE283K, αD335V, αD335N, αS337A, βD301T, βD301E, βR323M, and βR323K. This suggests that these mutants required more bonds to be made and broken during the rate-limiting step. In most of the mutations, the changes in $\Delta H^{\ddagger}$ and $T\Delta S^{\ddagger}$ resulted in lower k_{cat} values. However, in mutations αP279A/P280A, R282L, and βR323F, the changes in $\Delta H^{\ddagger}$ and $T\Delta S^{\ddagger}$ were compensated almost exactly such that k_{cat} remained unchanged. A higher k_{cat} was observed with βD301N because the decrease in $\Delta H^{\ddagger}$ was not compensated by a proportional change in $T\Delta S^{\ddagger}$. The mutation βR323L had the same $\Delta H^{\ddagger}$ and $T\Delta S^{\ddagger}$ values as XL10 and thus had the same k_{cat}.

For the rate-limiting step of a reaction, a linear free energy isokinetic relationship exists between rate constants (k_1 and k_2) measured at two temperatures ($T_2 > T_1$) such that

$$\log k_2 = a + b \log k_1 \quad (4)$$

where a and b are experimental constants (*15*). Treatments

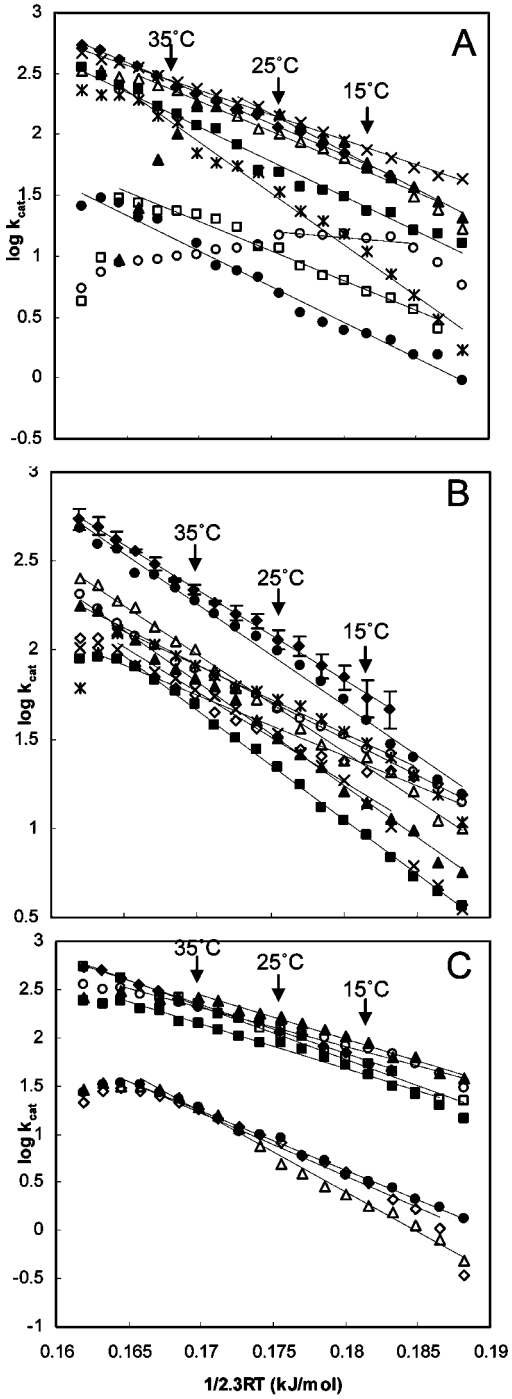

FIGURE 2: Arrhenius analysis of Mg-ATPase activity catalyzed by purified soluble (A) XL10-F_1 (◆), αP279G/P280G-F_1 (×), αP279A/P280A-F_1 (∗), αR282L-F_1 (△), αR282Q-F_1 (○), αR282K-F_1 (▲), αE283V-F_1 (□), αE283Q-F_1 (■), and αE283K-F_1 (●), (B) XL10-F_1 (◆), αD335V-F_1 (■), αD335T-F_1 (◇), αD335N-F_1 (▲), αD335E-F_1 (△), αS337A-F_1 (●), αS337V-F_1 (∗), αS337C-F_1 (○), and αS337D-F_1 (×), and (C) XL10-F_1 (◆), βD301T-F_1 (◇), βD301N-F_1 (▲), βD301E-F_1 (△), βR323L-F_1 (□), βR323F-F_1 (○), βR323M-F_1 (■), and βR323K-F_1 (●). The k_{cat} values were determined using 2 mM Mg^{2+}−ATP by the coupled assay as described in Experimental Procedures. Data points represent mean values from multiple analyses of each strain. Linear relations were generated by least-squares regression analysis of the data. The percent error of the data for XL10-F_1 is shown in panel B and was comparable to the percent error in the data obtained from the mutants.

that change the reaction rate but do not change the rate-limiting step of the reaction will correlate to a single linear relationship. The isokinetic plot in Figure 4 shows a linear correlation between the experimental ATP hydrolysis rate constants of most of the mutants with the XL10 derived at 15 and 25 °C. The exceptions were αP289G/P290G, βD301E, βR323K, and αR282Q which did not fall on the line, suggesting that these mutations changed the rate-limiting step of the reaction.

Table 4: Comparison of Thermodynamic Values at 25 °C for Mg^{2+}−ATP Hydrolysis Catalyzed by F_1 Isolated from XL10 and Mutants

strain	E_a (kJ/mol)	$\Delta H^{\ddagger}$ (kJ/mol)	$T\Delta S^{\ddagger}$ (kJ/mol)	$\Delta G^{\ddagger}$ (kJ/mol)
XL10	54.5	52.0	−9.2	61.2
αD335V	60.4	57.9	−7.4	65.3
αD335T	33.0	30.5	−33.6	64.1
αD335N	58.6	56.2	−8.3	64.5
αD335E	54.2	51.7	−11.7	63.4
αS337A	56.5	54.1	−7.8	61.9
αS337V	37.4	34.9	−29.0	63.9
αS337C	42.1	39.6	−24.0	63.6
αS337D	48.3	45.8	−19.2	64.9
βD301T	64.4	62.0	−6.1	68.1
βD301N	46.4	44.0	−16.6	60.6
βD301E	83.2	80.8	12.2	68.5
βR323L	55.1	52.6	−8.9	61.5
βR323F	41.1	38.6	−22.5	61.1
βR323M	46.4	43.9	−18.4	62.3
βR323K	60.8	58.3	−9.6	67.8
αP279G/P280G	79.4	76.9	12.5	64.4
αP279A/P280A	41.0	38.6	−22.2	60.8
αR282L	49.7	47.3	−14.3	61.6
αR282Q	6.7	4.2	−62.0	66.3
αR282K	65.1	62.6	1.8	60.7
αE283V	50.0	47.5	−19.8	67.3
αE283Q	57.2	54.7	−8.3	63.0
αE283K	59.6	57.2	−11.6	68.8

Mg^{2+}−ADP−Fluoroaluminate Inhibition. A tightly bound inhibitory complex forms at catalytic sites between F_1 and the Mg^{2+}−ADP−AlF_n species (*16*−*18*). Figure 5 shows the loss of ATPase activity in the presence of the Mg^{2+}−ADP−AlF_n species as a function of time. The isolated F_1 was incubated with 2 mM $MgCl_2$ and either 200 μM ADP or 1 molar equiv of ADP per F_1 for 1 h followed by addition of 50 μM $AlCl_3$ and 10 mM NaF for the indicated time period. The rates of inactivation approximated first-order processes such that first-order rate constants were compared (Table 5). Remarkably, αS337D preincubated with 1 molar equiv of ADP was more susceptible to inhibition than XL10 by 1 order of magnitude. Susceptibility also increased with αD335T, αD335E, αS337V, αS337C, βD301E, βR323K, E283V, and αE283K. Similar increases were also observed after preincubation with 200 μM ADP. A decreased susceptibility to Mg^{2+}−ADP−AlF_n inhibition was observed after preincubation with 200 μM ADP with αD335V, αD335N, αS337A, βD301T, βR323L, βR323F, and βR323M. Of these mutants, βD301T was least susceptible to Mg^{2+}−ADP−AlF_n inhibition, with a 2-fold decrease compared to that of XL10. With 1 molar equiv of ADP, smaller decreases in susceptibility were observed with this set of mutants.

DISCUSSION

The effects of the mutations presented here on ATPase activity strongly suggest that the hydrogen bonds connecting αD335, αS337, and βD301 that form when MgATP is bound

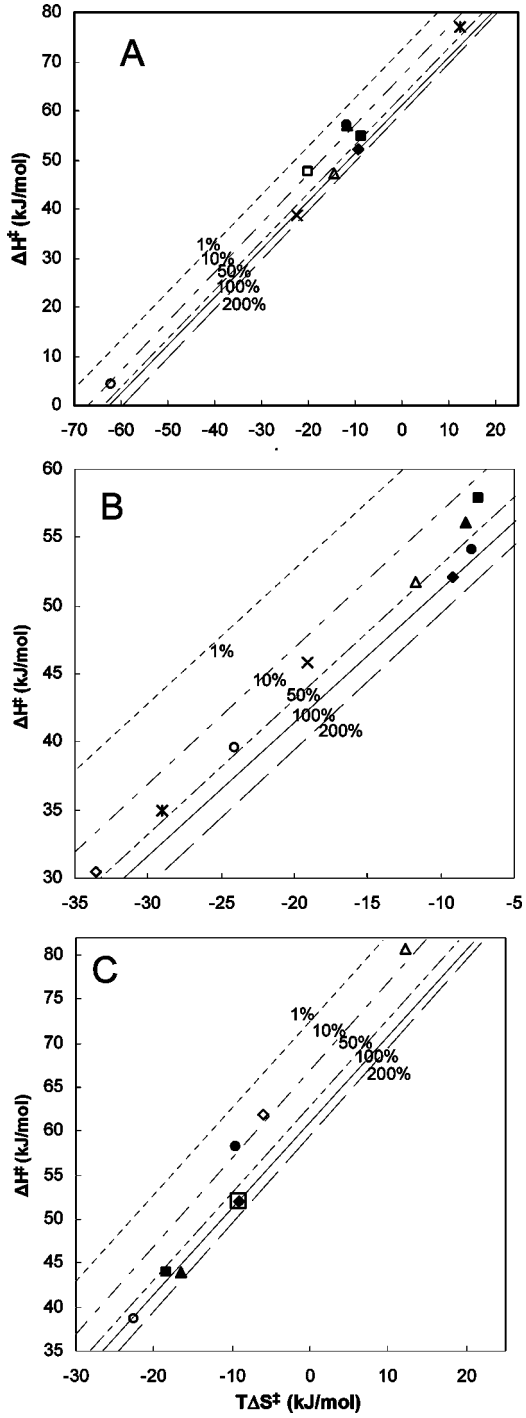

FIGURE 3: Free energy plot of Mg^{2+}-ATPase activity catalyzed by soluble F_1. Values for $\Delta H^{\ddagger}$, $T\Delta S^{\ddagger}$, and $\Delta G^{\ddagger}$ were derived at 25 °C from the Arrhenius data in Figure 2 using eqs 1−3: (A) XL10-F_1 (◆), αP279G/P280G-F_1 (∗), αP279A/P280A-F_1 (×), αR282L-F_1 (△), αR282Q-F_1 (○), αR282K-F_1 (▲), αE283V-F_1 (□), αE283Q-F_1 (■), and αE283K-F_1 (●), (B) XL10-F_1 (◆), αD335V-F_1 (■), αD335T-F_1 (◇), αD335N-F_1 (▲), αD335E-F_1 (△), αS337A-F_1 (●), αS337V-F_1 (∗), αS337C-F_1 (○), and αS337D-F_1 (×), and (C) XL10-F_1 (◆), βD301T-F_1 (◇), βD301N-F_1 (▲), βD301E-F_1 (△), βR323L-F_1 (□), βR323F-F_1 (○), βR323M-F_1 (■), and βR323K-F_1 (●). Isobars for $\Delta G^{\ddagger}$ are shown as lines that are the percentages of the indicated XL10 k_{cat} values.

to the catalytic site (Figure 1B) are important for catalytic function. Mutations which eliminated the ability to form these hydrogen bonds eliminated or significantly reduced ATP hydrolysis activity. The hydrogen bond connecting αE283 to αY339 in this conformation and in the EA conformation (Figure 1E) is also important, as supported by the decrease in ATPase activity caused by mutations which weakened or eliminated the ability of αE283 to form hydrogen bonds. Some mutations of βD301, βR323, and αR282 change the rate-limiting step of the enzyme.

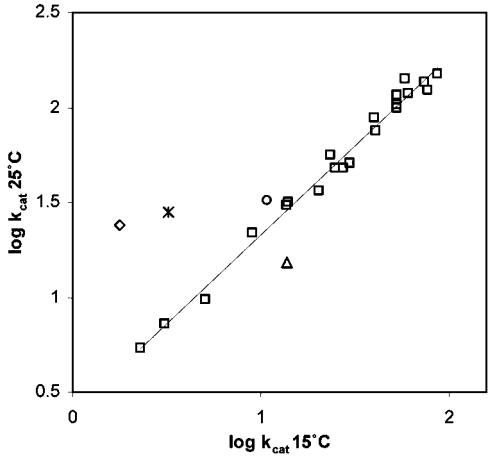

FIGURE 4: Isokinetic plot of log k_{cat} at 20 °C vs k_{cat} at 15 °C of Mg^{2+}-ATPase activity catalyzed by soluble F_1. All mutations are represented as □ except αR282Q (△), αP289G/P290G (○), βD301E (◇), and βR323K (∗).

Structural Basis for Changes in Hydrogen Bonds during Catalysis. A sequential ATPase mechanism can be constructed from conformations of the catalytic site with different nucleotide occupancies found in available crystal structures (Figure 1). In the EA conformation of (ADP)(AMPPNP)F_1 (Figure 1A), residues βD302, βT304, and βD305 of the catch loop (β301−305) are engaged with the γ subunit through hydrogen bonds and salt bridges. As shown in the FB conformation of (ADP)(AMPPNP)F_1 (Figure 1B), the binding of Mg^{2+}−ATP to the catalytic site induces the catch loop to form an alternate set of hydrogen bonds and salt bridges with residues in the α and β subunits such that these subunits move closer together. Catch loop residues βD302 and βD305 form salt bridges with αR282, and βD301 forms a salt bridge with βR323 and a hydrogen bond with αS337 (Figure 1B inset). Also, hydrogen bonds form between the backbone amine of αS337 and αD335 and between αE283 and the backbone amine of αY339. Residues αD335, αS337, and αY339 are connected to the nearby VISIT sequence (α344−348) by a short α helix. The VISIT sequence forms hydrogen bonds with βR182 and αR376 which engage the γ-phosphate of ATP. These arginines are known to be critical for the stabilization of the catalytic transition state (*6*−*8*, *19*), and the movement of phosphate away from ADP (*9*).

Events Concurrent with the First 120° Rotation. Comparison of the FB conformation of (ADP)(AMPPNP)F_1 to $(ADP{\cdot}AlF_4^-)_2F_1$ (Figure 1B,C) suggests that, as catalysis progresses, the hydrogen bonds connecting αS337 to βD301 and βR323, αD335 to αS337, and αE283 to αY339 dissociate upon formation of the transition state analogue complex. This is likely to be concurrent with a 120° rotation of the γ subunit, possible now that the catch loop residues have released their hydrogen bonds and salt bridges to the γ subunit. In the FB conformation of $(ADP{\cdot}AlF_4^-)_2F_1$ (Figure 1C), αR376 and βR182 are bound to the phosphate analogue,

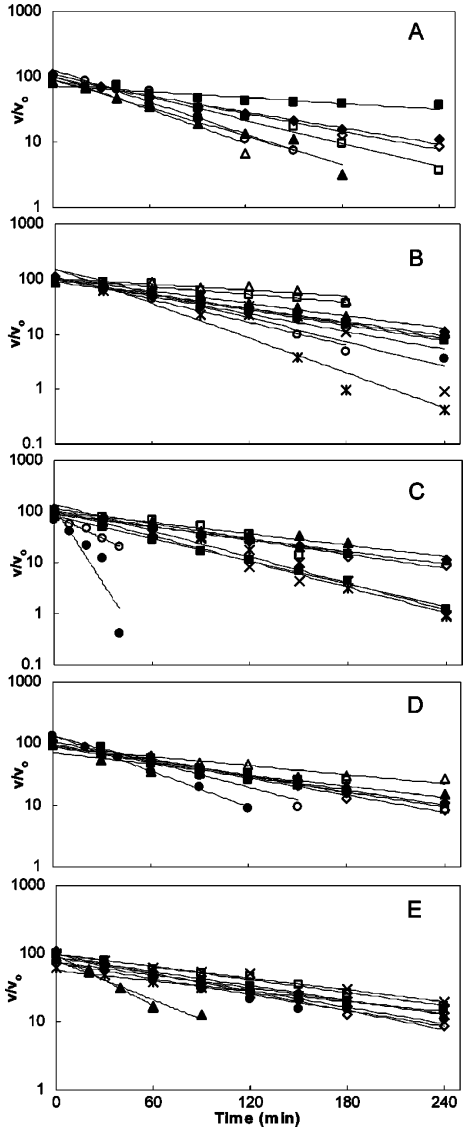

FIGURE 5: Inhibition by 50 μM AlF_n of Mg^{2+}-ATPase activity catalyzed by soluble F_1 at the indicated times after preincubation for 60 min with 2 mM $MgCl_2$ and 1 molar equiv of ADP to F_1 (filled symbols) or 2 mM $MgCl_2$ and 200 μM ADP (empty symbols). After preincubation for 1 h, 10 mM NaF and 50 μM $AlCl_3$ were added, and the sample was assayed for Mg^{2+}-ATPase activity. The log of v/v_o as a function of time after addition of NaF and $AlCl_3$ is plotted. The rate, v, is the rate at the indicated time after addition of 50 μM $AlCl_3$ and 10 mM NaF to a sample containing either 1 molar equiv of or 200 μM ADP, as indicated, and 2 mM $MgCl_2$. The rate, v_o, is the rate of a sample containing Mg^{2+}−ADP in one catalytic site, but in the absence of Al^{3+} and F^-. (A) One molar equivalent of ADP: XL10-F_1 (◆), αE283V-F_1 (▲), αE283Q-F_1 (■), and αE283K-F_1 (●); 200 μM ADP: XL10-F_1 (◇), αE283V-F_1 (△), αE283Q-F_1 (□), and αE283K-F_1 (○). (B) One molar equivalent of ADP: XL10-F_1 (◆), αD335V-F_1 (▲), αD335N-F_1 (■), αD335T-F_1 (●), and αD335E-F_1 (×); 200μM ADP: XL10-F_1 (◇), αD335V-F_1 (△), αD335N-F_1 (□), αD335T-F_1 (○), and αD335E-F_1 (∗). (C) One molar equivalent of ADP: XL10-F_1 (◆), αS337D-F_1 (●), αS337C-F_1 (■), αS337V-F_1 (×), and αS337A-F_1 (▲); 200 μM ADP: XL10-F_1 (◇), αS337D-F_1 (○), αS335C-F_1 (□), αS337V-F_1 (∗), and αS337A-F_1 (△). (D) One molar equivalent of ADP: XL10-F_1 (◆), βD301T-F_1 (▲), βD301N-F_1 (■), and βD301E-F_1 (●); 200 μM ADP: XL10-F_1 (◇), βD301T-F_1 (△), βD301N-F_1 (□), and βD301E-F_1 (○). (E) One molar equivalent of ADP: XL10-F_1 (◆), βR323K-F_1 (▲), βR323M-F_1 (■), βR323L-F_1 (●), and βR323F-F_1 (×); 200 μM ADP: XL10-F_1 (◇), βR323K-F_1 (△), βR323M-F_1 (□), βR323L-F_1 (○), and βR323F-F_1 (∗).

Table 5: Comparison of Rates of Formation of the Mg^{2+}−ADP−Fluoroaluminate Complexes Catalyzed by Isolated F_1

	equimolar ADP		200 μM ADP	
strain	k_{inact} ($\times 10^{-3}$ min^{-1})	% XL10	k_{inact} ($\times 10^{-3}$ min^{-1})	% XL10
XL10	9.4	100	10.6	100
αD335V	8.9	96	8.1	76
αD335T	17.0	183	16.0	151
αD335N	10.2	110	6.0	57
αD335E	16.3	175	25.9	244
αS337A	8.5	91	8.0	75
αS337V	19.6	211	17.5	165
αS337C	16.3	175	10.3	97
αS337D	129.4	1390	38.7	365
βD301T	6.9	74	5.6	53
βD301N	10.8	116	9.3	88
βD301E	28.2	303	16.0	151
βR323L	8.9	96	7.3	69
βR323F	7.0	75	6.9	65
βR323M	7.9	85	7.3	69
βR323K	17.4	187	31.8	300
αE283V	17.2	185	31.6	298
αE283Q	2.9	31	11.8	111
αE283K	13.6	146	17.4	176

and only βR182 remains bound to the VISIT sequence through αI347 and αT348.

The rate-limiting step for the F_1 ATPase is product release, rather than transition state formation (*20*). Consequently, a change in stability of the transition state induced by a mutation may not result in a lower k_{cat} unless this step becomes rate-limiting. However, Mg^{2+}−ADP−fluoroaluminate inhibition provides an estimate of transition state stability. Results presented here show that the hydrogen bonds connecting βD301, βR323, and αS337, as well the hydrogen bond connecting the backbone amine of αS337 to αD335, are important for transition state stabilization (Figure 1B). The αS337D mutation greatly increased the susceptibility to Mg^{2+}−ADP−fluoroaluminate inhibition and lowered the k_{cat} of ATP hydrolysis. The αS337D mutation would replace the native hydrogen bond to βR323 with a salt bridge and repel the negatively charged βD301. Increased susceptibility to Mg^{2+}−ADP−fluoroaluminate inhibition and lowered ATPase rates were also observed with the conservative mutations αD335E, βD301E, and βR323K that primarily alter the size of the side chains. In contrast, eliminating or weakening the ability to form these hydrogen bonds with the αS337A, βD301T, αD335V, and αD335N mutations resulted in a decreased susceptibility to Mg^{2+}−ADP−fluoroaluminate inhibition and a lowered k_{cat} for ATP hydrolysis. Though both βD335N and βD335T weaken the ability of this residue to form a hydrogen bond, only βD335N lowered the susceptibility to Mg^{2+}−ADP−fluoroaluminate inhibition.

Though αS337A lowered the susceptibility to Mg^{2+}−ADP−fluoroaluminate inhibition and slightly lowered the k_{cat}, the similar but slightly larger substitution αS337V increased the susceptibility to Mg^{2+}−ADP−fluoroaluminate inhibition and lowered ATPase rates, indicating that the introduction of steric hindrance affected the VISIT position. The βR323L, βR323F, and βR323M mutations, which affected the ability to form the salt bridge and hydrogen bond to βD301 and αS337, decreased the susceptibility to Mg^{2+}−ADP−fluoroaluminate inhibition, although the k_{cat} of ATPase was not affected. This suggests that the interactions of βR323

with βD301 and αS337 are important to transition state stabilization, again through influence on the VISIT sequence position, and subsequently on catalytic residues βR182 and αR376, the arginine finger (Figure 1B,C).

The results of the mutations to βD301, βR323, αS337, and αD335 suggest that the hydrogen bonds and salt bridges in which these residues participate are important for the proper alignment of the VISIT sequence, which interacts with both βR182 and αR376, the arginine finger, at the catalytic site. In Figure 1B, βR182 forms hydrogen bonds to αI345, αI348, and αT348, while αR376 hydrogen bonds to αT348. These arginines are critical to the stabilization of the catalytic transition state (*6*−*9*, *19*). Thus, the hydrogen bonds connecting βD301 to both βR323 and αS337, and the backbone amine of αS337 to αD335, provide a short link between the rotational position of the γ subunit and the conformation of the catalytic sites.

Events Concurrent with the Second 120° Rotation. When the FB and DC conformations of $(ADP{\cdot}AlF_4^-)_2F_1$ are compared (Figure 1C,D), the phosphate moves away from the ADP. Catalytic residues βR182 and αR376, the arginine finger, also move, changing their hydrogen bond connections to VISIT as well as to ADP and P_i. In Figure 1D, βR182 remains hydrogen bonded to αI347 and αT348, and αR376 is now hydrogen bonded to αI345. The αR282−βD305 salt bridge also dissociates. This may be concurrent with a second 120° rotation of the γ subunit.

The αR282−βD305 salt bridge that forms upon conversion of the low- to high-affinity site (Figure 1B) and dissociates in Figure 1C appears to be very important to the function of the enzyme. The αR282Q mutation changes the rate-limiting step of the reaction (Figure 4), which appears to be temperature-dependent, as is evident in the break in the Arrhenius plot (Figure 2). This mutant also decreased the number of interactions during the rate-limiting step (Figure 3). Mutations βD305V and βD305S do not assemble, and the k_{cat} of the conservative βD305E mutation is only 4% of that of the wild-type enzyme (*5*).

Events Concurrent with the Final 120° Rotation. The EA conformation of the $(ADP{\cdot}AlF_4^-)_2F_1$ structure (Figure 1E) contains Mg^{2+}−ADP and sulfate. In this conformation, βR323 has formed a hydrogen bond to αS371 in lieu of the salt bridge with βD301. It was previously suggested that the β subunit changes its conformation upon phosphate release, based upon results of a tryptophan substitution used to follow the movement of βR323 (*21*). In this conformation, catch loop residues βD302 and βD305 have also formed salt bridges to γQ269 and γR268, consistent with a γ subunit rotational event. Since product release is thought to be a prerequisite for the final 30° rotational substep (Figure 1, frame E → frame A) (*22*−*25*), and the foot of $(ADP{\cdot}AlF_4^-)_2F_1$ is rotated ∼20° from that in $(ADP)(AMPPNP)F_1$, this may result from a 90° rotational substep (Figure 1, frame D → frame E). The catalytic arginines βR182 and αR376 coordinate the phosphate analogue, sulfate, and a hydrogen bond now connects αR376 to αT348 of VISIT while βR182 is not bound to the VISIT sequence. The hydrogen bond connecting αE283 to αY339 has formed again as in Figure 1B, allowing αE283 to influence the position of the VISIT sequence during the rate-limiting product release step. The presence of this hydrogen bond in both the FB and EA conformations (Figure 1B,E) may explain the results with the αE283V and αE283K mutations. Both αE283V and αE283K resulted in higher susceptibilities to Mg^{2+}−ADP−fluoroaluminate inhibition and lowered ATP hydrolysis activity by 2 orders of magnitude, suggesting that loss of the ability to form the hydrogen bond to αY339 stabilized the transition state and slowed product release. The importance of correct positioning of αE283 is suggested by the effects of the αP279G/P280G mutant, which would introduce flexibility into the loop containing αE283. This double mutant, which lowered k_{cat} and decreased lactate- and ATP-dependent proton pumping, appeared to change the rate-limiting step (Figure 4).

The importance of the alignment of the VISIT sequence and subsequently the interactions of catalytic residues αR376 and βR182 with the nucleotide is supported by the results of several other mutations. The Arrhenius analysis and free energy plot results presented here indicate that αD335V, αD335N, and αS337A form more interactions and hydrogen bonds in their rate-limiting step than XL10. These mutations also decreased the susceptibility to Mg^{2+}−ADP−fluoroaluminate inhibition. The opposite effects were observed with αD335E, αD335T, αS337D, and αS337V, which had weakened interactions in their rate-limiting step and stronger Mg^{2+}−ADP−fluoroaluminate inhibition.

The isokinetic plot (Figure 4) clearly indicates that the conservative mutations βD301E and βR323K cause a change in the rate-limiting step for ATP hydrolysis. These mutations also increased the number of interactions during the rate-limiting step (Figure 3) and increased the susceptibility to Mg^{2+}−ADP−fluoroaluminate inhibition (Table 5). Residues βD301 and βR323 form a salt bridge in both the FB and DC states (Figure 1B−D), which is broken in the EA state upon product release. These conservative mutations primarily change the length of these residues and may cause a step prior to product release to become rate-limiting. In contrast, the other mutations to βD301 and βR323 did not indicate a change in the rate-limiting step, either decreased or had little effect on the susceptibility to Mg^{2+}−ADP−fluoroaluminate inhibition, and had variable effects on the free energy plot.

Hydrogen Bonds Important to ATP Synthesis. The rotation of γ during ATP synthesis has been suggested to be controlled by an escapement mechanism (*4*, *5*, *10*, *26*). In this mechanism, rotation is prevented until the empty catalytic site binds substrate. The hydrogen bonds and salt bridges connecting γ to the surrounding $(\alpha\beta)_3$ ring are then broken, allowing γ subunit rotation in response to the constant torque from the proton gradient. Binding of MgATP triggers the formation of an alternate set of hydrogen bonds to the catch loop at the interface of the α and β subunits (Figure 1B). Results presented here show that mutations which eliminate or weaken hydrogen bonds formed by catch loop residues βD301, αD335, and αE283 in this alternative conformation decrease the rates of ATP synthase-dependent growth and lactate-dependent proton gradient formation. These results suggest that the roles of βD301, αD335, and αE283 in forming the catch loop alternate structure are important in permitting the release of intersubunit bonds which would allow γ rotation.

Hydrogen Bonds Important to ATP Hydrolysis. Previous results suggest that the rotation of the γ subunit is induced by the pull of surrounding β subunit side chains which form intersubunit bonds to γ residues, including those connecting

γT273 and γE275 to βV265 and γR9 to D386 (*10*, *26*). Available crystal structures show hydrogen bonds or salt bridges connecting γT273 and γE275 to βV265 and γR9 to βD386. Further inductive force on the γ subunit could be generated by similarly positioned residues of the α subunit. As the catalytic site transitions from the DC to EA conformation (Figure 1, frame D → frame E), a 90° rotation of the γ subunit may be induced by salt bridges that likely form as γK266 and γR268 come within van der Waals contact of αD335, though these salt bridges are not shown in any available crystal structures. It has previously been suggested that the movements of catalytic residues αR376 and βR182 are transmitted through the α subunit to communicate the status of the catalytic site to the γ subunit (*7*, *8*). We suggest that these $\alpha-\gamma$ interactions may contribute Coulombic potential to generate an inductive force that could drive γ subunit rotation. The lower ATPase activity of hydrophobic and polar substitutions at the αD335 position may result if the $\alpha-\gamma$ subunit interactions contribute to the mechanism that converts ATP binding and hydrolysis into rotational motion of the γ subunit. These interactions would need to work in concert with other similar $\alpha-\gamma$ or $\beta-\gamma$ subunit interactions that come into van der Waals contact at different rotational positions of the γ subunit.

REFERENCES

1. Abrahams, J. P., Leslie, A. G., Lutter, R., and Walker, J. E. (1994) Structure at 2.8 Å resolution of F1-ATPase from bovine heart mitochondria, *Nature 370*, 621−8.
2. Braig, K., Menz, R. I., Montgomery, M. G., Leslie, A. G., and Walker, J. E. (2000) Structure of bovine mitochondrial F_1-ATPase inhibited by Mg^{2+}, ADP and aluminium fluoride, *Structure 8*, 567−73.
3. Menz, R. I., Walker, J. E., and Leslie, A. G. (2001) Structure of bovine mitochondrial F_1-ATPase with nucleotide bound to all three catalytic sites: Implications for the mechanism of rotary catalysis, *Cell 106*, 331−41.
4. Chen, W., and Frasch, W. D. (2001) Interaction of the catch-loop tyrosine βY317 with the metal at catalytic site 3 of *Chlamydomonas* chloroplast F1-ATPase, *Biochemistry 40*, 7729−35.
5. Greene, M. D., and Frasch, W. D. (2003) Interactions among γR268, γQ269, and the β subunit catch loop of *Escherichia coli* F1-ATPase are important for catalytic activity, *J. Biol. Chem. 278*, 51594−8.
6. Nadanaciva, S., Weber, J., Wilke-Mounts, S., and Senior, A. E. (1999) Importance of F1-ATPase residue α-Arg-376 for catalytic transition state stabilization, *Biochemistry 38*, 15493−9.
7. Weber, J., Nadanaciva, S., and Senior, A. E. (2000) ATP-driven rotation of the γ subunit in F_1-ATPase, *FEBS Lett. 483*, 1−5.
8. Le, N. P., Omote, H., Wada, Y., Al-Shawi, M. K., Nakamoto, R. K., and Futai, M. (2000) *Escherichia coli* ATP synthase α subunit Arg-376: The catalytic site arginine does not participate in the hydrolysis/synthesis reaction but is required for promotion to the steady state, *Biochemistry 39*, 2778−83.
9. Ahmad, Z., and Senior, A. E. (2005) Involvement of ATP synthase residues αArg-376, βArg-182, and βLys-155 in P_i binding, *FEBS Lett. 579*, 523−8.
10. Boltz, K. W., and Frasch, W. D. (2005) Interactions of γT273 and γE275 with the β Subunit PSAV Segment that Links the γ Subunit to the Catalytic Site Walker Homology B Aspartate Are Important to the Function of *Escherichia coli* F_1F_o ATP Synthase, *Biochemistry 44*, 9497−506.
11. Senior, A. E., Latchney, L. R., Ferguson, A. M., and Wise, J. G. (1984) Purification of F1-ATPase with impaired catalytic activity from partial revertants of *Escherichia coli* uncA mutant strains, *Arch. Biochem. Biophys. 228*, 49−53.
12. Kato, Y., Sasayama, T., Muneyuki, E., and Yoshida, M. (1995) Analysis of time-dependent change of *Escherichia coli* F1-ATPase activity and its relationship with apparent negative cooperativity, *Biochim. Biophys. Acta 1231*, 275−81.
13. Al-Shawi, M. K., and Senior, A. E. (1988) Complete kinetic and thermodynamic characterization of the unisite catalytic pathway of *Escherichia coli* F1-ATPase. Comparison with mitochondrial F1-ATPase and application to the study of mutant enzymes, *J. Biol. Chem. 263*, 19640−8.
14. Futai, M., Sternweis, P. C., and Heppel, L. A. (1974) Purification and properties of reconstitutively active and inactive adenosinetriphosphatase from *Escherichia coli*, *Proc. Natl. Acad. Sci. U.S.A. 71*, 2725−9.
15. Exner, O. (1973) The enthalpy-entropy relationship, *Prog. Phys. Org. Chem. 10*, 411−82.
16. Dou, C., Grodsky, N. B., Matsui, T., Yoshida, M., and Allison, W. S. (1997) ADP-fluoroaluminate complexes are formed cooperatively at two catalytic sites of wild-type and mutant $\alpha_3\beta_3\gamma$ subcomplexes of the F-1-ATPase from the thermophilic *Bacillus* PS3, *Biochemistry 36*, 3719−27.
17. Allison, W. S., Ren, H., and Dou, C. (2000) Inhibitory Mg-ADP-Fluoroaluminate Complexes Bound to Catalytic Sites of F1-ATPases: Are They Ground-State or Transition-State Analogs? *J. Bioenerg. Biomembr. 32*, 531−8.
18. Nadanaciva, S., Weber, J., and Senior, A. E. (1999) Binding of the transition state analog MgADP-fluoroaluminate to F1-ATPase, *J. Biol. Chem. 274*, 7052−8.
19. Nadanaciva, S., Weber, J., and Senior, A. E. (1999) The role of β-Arg-182, an essential catalytic site residue in *Escherichia coli* F1-ATPase, *Biochemistry 38*, 7670−7.
20. Boyer, P. D. (1993) The binding change mechanism for ATP synthase−some probabilities and possibilities, *Biochim. Biophys. Acta 1140*, 215−50.
21. Masaike, T., Muneyuki, E., Noji, H., Kinosita, K., Jr., and Yoshida, M. (2002) F1-ATPase changes its conformations upon phosphate release, *J. Biol. Chem. 277*, 21643−9.
22. Sakaki, N., Shimo-Kon, R., Adachi, K., Itoh, H., Furuike, S., Muneyuki, E., Yoshida, M., and Kinosita, K., Jr. (2005) One rotary mechanism for F1-ATPase over ATP concentrations from millimolar down to nanomolar, *Biophys. J. 88*, 2047−56.
23. Nishizaka, T., Oiwa, K., Noji, H., Kimura, S., Muneyuki, E., Yoshida, M., and Kinosita, K., Jr. (2004) Chemomechanical coupling in F1-ATPase revealed by simultaneous observation of nucleotide kinetics and rotation, *Nat. Struct. Mol. Biol. 11*, 142−8.
24. Shimabukuro, K., Yasuda, R., Muneyuki, E., Hara, K. Y., Kinosita, K., Jr., and Yoshida, M. (2003) Catalysis and rotation of F1 motor: Cleavage of ATP at the catalytic site occurs in 1 ms before 40° substep rotation, *Proc. Natl. Acad. Sci. U.S.A. 100*, 14731−6.
25. Yasuda, R., Noji, H., Yoshida, M., Kinosita, K., Jr., and Itoh, H. (2001) Resolution of distinct rotational substeps by submillisecond kinetic analysis of F1-ATPase, *Nature 410*, 898−904.
26. Lowry, D. S., and Frasch, W. D. (2005) Interactions between βD372 and γ subunit N-terminus residues γK9 and γS12 are important to catalytic activity catalyzed by *Escherichia coli* F1Fo-ATP synthase, *Biochemistry 44*, 7275−81.

BI052592+